DOCUMENTATION

of

BRAIN MEASURES

in

MIDUS 3
Neuroscience Project (P5)

University of Wisconsin ♦ Institute on Aging
February 2026

TABLE OF CONTENTS

INTRODUCTION

This document is an updated reference for the extracted structural and diffusion brain measures and metrics derived from brain-based aging algorithms from the MIDUS 3 Neuroscience Project data set. This document also includes information regarding the Neuroscience Project's (P5) MIDUS 3 MRI data collection and processing protocols.

Raw MRI data (including structural, task functional, resting functional, diffusion-weighted imaging, and resting perfusion) and associated behavioral data are available through a restricted access data sharing mechanism. Please see *M3_P5_RESTRICTED_ACCESS_20260106* and/or https://midus.wisc.edu/midus-neuroscience-repository/ for more information about what is available and instructions on how to access these data.

General information about MRI scans

All MIDUS 3 scans were performed at the Waisman Brain Imaging Laboratory on the UW-Madison campus using a 3T MR750 GE Healthcare MRI scanner (Waukesha, WI) and a 32-channel NOVA head coil. MRI scans typically took place during the morning of the second day of Neuroscience Project data collection (see **C5ITS** and **C5ITF** for the exact MRI start times). In total, the scanning protocol had a duration of approximately 90 minutes and included the acquisition of a BRAVO T1-weighted scan, field map images, 3 task functional MRI (fMRI) scans, a resting-state fMRI scan, a diffusion-weighted scan, and an arterial spin labeling scan. Additionally, T2 Cube and T2 Cube Flair scans were added to the end of the protocol, if time allowed, part way through the MIDUS 3 data collection. Questionnaire data, including PANAS-NOW and STAI-State, both prior to and after the scanning procedure, are also available (see *M3_P5_DOCUMENTATION_OF_PROCEDURES_20260206* and *M3_P5_DOCUMENTATION_OF_SCALES_20260206* for more information).

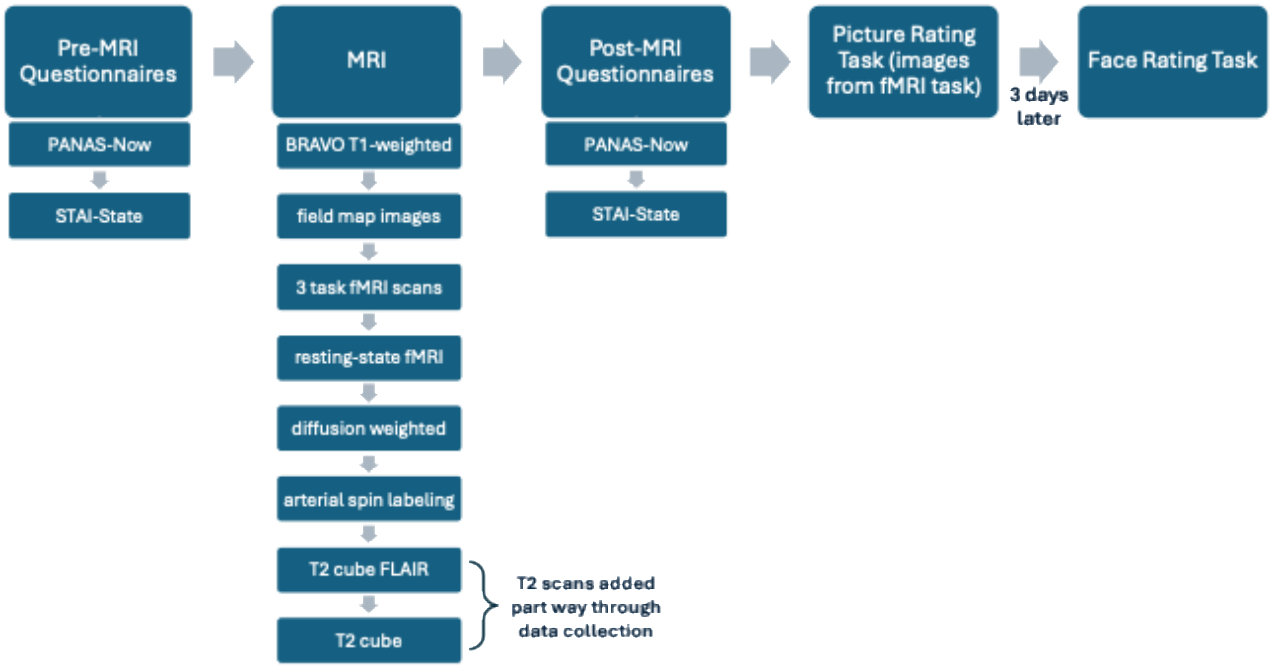

Partial variable names have been provided where appropriate. In partial variable names note that "_" represents a single character. For more detailed information on variable names see variable naming or atlas tables below or see *M3_P5_VARIABLE_NAMES_20260206*.

Differences Between MIDUS Waves

To aid in the comparison of data described in this document between waves, a brief description of the major differences across waves has been provided.

MIDUS 2 vs MIDUS 3

The Waisman Brain Imaging MRI scanner was updated between the MIDUS 2 and MIDUS Refresher 1 data collections. Due to limitations in scan quality at the time of MIDUS 2 data collection (which suffered a severe intensity bias that so far has not been able to be corrected with bias corrections), the MIDUS 2 structural data was of insufficient quality to provide these estimates from the structural MRI data. Additionally, diffusion-weighted scanning was not performed at MIDUS 2. Therefore, extracted structural and diffusion brain measures and metrics derived from brain-based aging algorithms are only available in MIDUS Refresher 1 and MIDUS 3.

MIDUS Refresher 1 vs MIDUS 3

In MIDUS Refresher 1 an 8-channel head coil was used, but in MIDUS 3 it was swapped for a 32-channel NOVA head coil.

The diffusion-weighted imaging (DWI) acquisitions differed between MIDUS Refresher 1 and MIDUS 3 data collections. Although both MIDUS Refresher 1 and MIDUS 3 have multi-shell DWI data and have extracted diffusion tensor estimates (DTI: FA, MD, AD, RD), those measures should not be combined across MIDUS Refresher 1 and MIDUS 3 without appropriate harmonization of the data. Moreover, the higher diffusion weighting in MIDUS 3 DWI acquisition allowed additional models (DKI, WMTI, NODDI) and their estimates to be computed and extracted.

Scan Data Quality Filters

A subset of the participants who completed the Neuroscience Psychophysiology protocol completed the MRI protocol. In some cases, data could not be collected due to claustrophobia, back problems, or other issues that prevented the participant from completing the MRI scan. A filter variable is provided, indicating whether participants completed a T1-weighted scan **[C5IC]**. However, a small number of scans contained artifacts that made accurate structural measurements unfeasible. In all cases, the appropriate missing value was listed. A second filter indicates whether a radiologist flagged the scan for an abnormality during review **[C5IF]**. Radiologist flags were most typically indicating small vessel ischemic disease, presence of meningiomas or other masses, and/or referrals to specialists. Please note that the radiologist only flagged scans with unexpected findings. If a participant self-reported a health concern that could explain an otherwise unusual scan, the scan would not be flagged by the radiologist. Therefore, an additional variable of self-reported neurological condition has been provided **[C5IN]** to accompany the radiologist flag. The self-reported neurological conditions may include seizure disorders, Parkinson's, tremors, multiple sclerosis, Alzheimer's disease or related dementia, previous stroke/TIA, brain aneurysm, head/brain injury, cyst on the brain, or other condition (unclear if central or peripheral nervous system condition). In addition to the self-reported neurological conditions, the radiologist would have taken into account other self-reported chronic medical conditions such as

diabetes, asthma, hypertension, cancer, and other diseases not listed here which could have affected the brain in ways expected for those conditions typically indicative of accelerated brain aging.

FREESURFER-EXTRACTED STRUCTURAL BRAIN MEASUREMENTS

Scanning parameters: BRAVO T1-weighted (T1w) structural images with 1 mm^3 isotropic voxels (TR = 8.2 ms, TE = 3.2 ms, flip angle = 12°, FOV = 256 mm, 256 x 256 matrix, 156 axial slices, inversion time = 450 ms, total duration = 7.5 minutes).

FreeSurfer processing: Cortical reconstruction and volumetric segmentation was performed with the FreeSurfer image analysis suite (v6.0.0), which is documented and freely available for download online (http://surfer.nmr.mgh.harvard.edu/). The technical details of these procedures are described in prior publications (Dale et al., 1999; Dale & Sereno, 1993; Fischl & Dale, 2000; Fischl et al., 2001; Fischl et al., 2002; Fischl et al., 2004a; Fischl et al., 1999a; Fischl et al., 1999b; Fischl et al., 2004b; Han et al., 2006; Jovicich et al., 2006; Segonne et al., 2004; Reuter et al., 2010; Reuter et al., 2012).

Briefly, this processing includes motion correction and removal of non-brain tissue using a hybrid watershed/surface deformation procedure (Segonne et al., 2004), automated Talairach transformation, segmentation of the subcortical white matter and deep gray matter volumetric structures (including hippocampus, amygdala, caudate, putamen, ventricles) (Fischl et al., 2002; Fischl et al., 2004a) intensity normalization (Sled et al., 1998), tessellation of the gray matter white matter boundary, automated topology correction (Fischl et al., 2001; Segonne et al., 2007), and surface deformation following intensity gradients to optimally place the gray/white and gray/cerebrospinal fluid borders at the location where the greatest shift in intensity defines the transition to the other tissue class (Dale et al., 1999; Dale & Sereno, 1993; Fischl & Dale, 2000). Once the cortical models are complete, a number of deformable procedures can be performed for further data processing and analysis including surface inflation (Fischl et al., 1999a), registration to a spherical atlas which is based on individual cortical folding patterns to match cortical geometry across subjects (Fischl et al., 1999b), parcellation of the cerebral cortex into units with respect to gyral and sulcal structure (Desikan et al., 2006; Fischl et al., 2004b; Klein & Tourville, 2012), and creation of a variety of surface based data including maps of curvature and sulcal depth. This method uses both intensity and continuity information from the entire three-dimensional MR volume in segmentation and deformation procedures to produce representations of cortical thickness, calculated as the closest distance from the gray/white boundary to the gray/CSF boundary at each vertex on the tessellated surface (Fischl & Dale, 2000). The maps are created using spatial intensity gradients across tissue classes and are therefore not simply reliant on absolute signal intensity. The maps produced are not restricted to the voxel resolution of the original data thus are capable of detecting submillimeter differences between groups. Procedures for the measurement of cortical thickness have been validated against histological analysis (Rosas et al., 2002) and manual measurements (Kuperberg et al., 2003; Salat et al., 2004). FreeSurfer morphometric procedures have been demonstrated to show good test-retest reliability across scanner manufacturers and across field strengths (Han et al., 2006; Reuter et al., 2012). Segmentation quality was visually assessed and manually edited as necessary (http://freesurfer.net/fswiki/Edits). After the manual edits segmentation of the hippocampal subfields and amygdala nuclei was performed using FreeSurfer v7.1.0. Description of these segmentations can be found in Iglesias et al. (2015) for the hippocampus and Saygin and Kliemann et al. (2017) for the amygdala.

Extracted FreeSurfer measures are provided for 159 participants

- Using FreeSurfer (v6.0.0) cortical parcellation was performed using 3 atlases to calculate measures of cortical thickness, curvature, surface area, and volume:
    - Destrieux atlas (Fischl et al., 2004b) **[C5E_ _D…]**
    - Desikan-Killiany atlas (Desikan et al., 2006) **[C5E_ _K…]**
    - Desikan-Killiany-Tourville (DKT) atlas (Klein & Tourville, 2012) **[C5E_ _T…]**
- Subcortical volumes **[C5ES_A…]** were derived via the
    - Automatic Segmentation (aseg) atlas (Fischl et al., 2002) – using FreeSurfer v6.0.0
    - Hippocampal and Amygdala segmentation modules performed using FreeSurfer v7.1.0
        - Hippocampal subfields (Iglesias et al., 2015)
        - Nuclei of the amygdala (Saygin & Kliemann et al., 2017)

Differences in FreeSurfer naming conventions between waves: For the MIDUS Refresher 1 wave, an aseg variable labeled as 'CorticalWhiteMatter' was extracted using FreeSurfer v5.3.0. For MIDUS 3, FreeSurfer v6.0.0 re-labeled that same aseg variable as 'CerebralWhiteMatter'. FreeSurfer creators thought 'CerebralWhiteMatter' was the better naming convention, but these variables reflect the same measure across waves.

BRAIN-BASED AGING ALGORITHMS

Scanning parameters: BRAVO T1-weighted (T1w) structural images with 1 mm^3 isotropic voxels (TR = 8.2 ms, TE = 3.2 ms, flip angle = 12°, FOV = 256 mm, 256 x 256 matrix, 156 axial slices, inversion time = 450 ms, total duration = 7.5 minutes).

Dunedin Pace of Aging Calculated from NeuroImaging (DunedinPACNI)

The DunedinPACNI is a computed measure of "the rate of longitudinal aging" derived from cross-sectional brain magnetic resonance imaging (Whitman et al., 2025).

Processing for DunedinPACNI: The output of the FreeSurfer parcellations was also used to derive the Dunedin Pace of Aging Calculated from NeuroImaging (DunedinPACNI) **[C5EBD]**. We ran the open source DunedinPACNI package at HEAD, commit 3760130 on T1-weighted MRI scans that were preprocessed and parcellated using FreeSurfer image analysis suite (v6.0.0). See the DunedinPACNI documentation for detailed information about the algorithm.

Whitman, E. T., Elliott, M. L., Knodt, A. R., Abraham, W. C., Anderson, T. J., Cutfield, N. J., Hogan, S., Ireland, D., Melzer, T. R., Ramrakha, S., Sugden, K., Theodore, R., Williams, B. S., Caspi, A., Moffitt, T. E., & Hariri, A. R. (2025). DunedinPACNI estimates the longitudinal Pace of Aging from a single brain image to track health and disease. *Nature aging*, *5*(8), 1619–1636. https://doi.org/10.1038/s43587-025-00897-z **PMID:** 40595015

GitHub link: https://github.com/etw11/DunedinPACNI

Brain-Predicted Age

Brain-predicted age was calculated using multiple publicly shared algorithms and deep learning models which have been pretrained with cross-validation on other external T1-weighted MRI datasets:

Cole Brainage Estimates

Cole brainageR v1.0 **[C5EB]** and Cole brainageR v2.0 **[C5EBC]** both using Gaussian Processes regression described in detail on https://github.com/james-cole/brainageR, which according to the GitHub description use similar but not identical methods as Cole, J. H., Leech, R., Sharp, D. J., & Initiative, A. D. N. (2015). Prediction of brain age suggests accelerated atrophy after traumatic brain injury. *Annals of Neurology*, *77*(4), 571–581. doi: 10.1002/ana.24367.

Processing for BrainAgeR v1.0 estimation: The software takes raw T1-weighted MRI scans, then uses SPM12 for segmentation and normalisation. A slightly customized version of FSL's slicesdir* is then used to generate a directory of PNGs and corresponding index.html file for quality controlling in a web browser. Finally, the normalised images are loaded into R using the RNfiti package, vectorised and grey matter, white matter, and CSF vectors masked (using 0.3 in the average image from the brainageR-specific template, derived from n=200 scans, n=20 from each of the n=10 scanners) and combined.

GitHub link - BrainAgeR v1.0: https://github.com/james-cole/brainageR/tree/1.0

Processing for BrainAgeR v2.0 estimation: In version 2.0 of Cole's software, Principal Components Analysis was run (using R's prcomp), and the top 80% of variance retained. This meant 435 PCs were included. The rotation matrix of the PCA is applied to any new data and these 435 variables are then used to predict an age value with the trained model with **kernlab**. The entailed using a GPR with RBF kernel and default hyperparameters.

GitHub link - BrainAgeR v2.0: https://github.com/james-cole/brainageR/tree/2.0

Citation information:

The GitHub details for Cole v1.0 and v2.0 include a request for R citation. "Since kernlab does most of the heavy lifting, please consider citing this excellent package: https://cran.r-project.org/web/packages/kernlab/citation.html."

"This model has yet to be used in a publication as of 30/09/2019, however some of the training dataset and general approach have been used before. So if you use this software, please consider citing one or more of the following papers:

Cole JH, Ritchie SJ, Bastin ME, Valdes Hernandez MC, Munoz Maniega S, Royle N et al. Brain age predicts mortality. Molecular psychiatry 2018; 23: 1385-1392.

Cole JH, Poudel RPK, Tsagkrasoulis D, Caan MWA, Steves C, Spector TD et al. Predicting brain age with deep learning from raw imaging data results in a reliable and heritable biomarker. NeuroImage 2017; 163C: 115-124.

Cole JH, Leech R, Sharp DJ, for the Alzheimer's Disease Neuroimaging Initiative. Prediction of brain age suggests accelerated atrophy after traumatic brain injury. Ann Neurol 2015; 77(4): 571-581."

However, it is important to note that none of these papers' methods exactly match the GitHub description, so they provide the gist but not exact details of the methods.

TSAN Brainage Estimates **[C5EBT] - PMID:** 34086565

The Two-Stage-Age-Net (TSAN) is an algorithm used to estimate brainage using T1-weighted MRI data.

Processing for TSAN estimation: Raw T1-weighted MRI scans were preprocessed following the guidelines presented in the GitHub repository for TSAN. The data were reoriented to the standard MNI orientation. The images were skull-stripped, and corrected for B1 bias using the

N4 algorithm implemented in ANTs. The data were then non-linearly registered to MNI 2 mm x 2 mm x 2 mm MNI skull stripped template. These preprocessed images were fed as input to the trained deep learning model described in these papers:

Cheng, J., Liu, Z., Guan, H., Wu, Z., Zhu, H., Jiang, J., Wen, W., Tao, D., & Liu, T. (2021). Brain Age Estimation From MRI Using Cascade Networks With Ranking Loss. *IEEE transactions on medical imaging*, *40*(12), 3400–3412. https://doi.org/10.1109/TMI.2021.3085948 **PMID:** 34086565

Liu, Z., Cheng, J., Zhu, H., Zhang, J., & Liu, T. (2020). Medical Image Computing and Computer Assisted Intervention – MICCAI 2020, 23rd International Conference, Lima, Peru, October 4–8, 2020, Proceedings, Part VII. *Lecture Notes in Computer Science*, 198–207. https://doi.org/10.1007/978-3-030-59728-3_20

GitHub link: TSAN-brain-age-estimation: TSAN: Two-Stage-Age-Net, for brain age estimation from T1-weighted MRI data https://github.com/Milan-BUAA/TSAN-brain-age-estimation

3D-CNN Brainage Estimates **[C5EBP] - PMID:** 36595679

The three-dimensional convolution neural network (3D-CNN) is an algorithm used to estimate brainage using T1-weighted MRI data.

Processing for 3D-CNN estimation: Raw T1-weighted MRI scans were preprocessed with the FreeSurfer image analysis suite (v6.0.0), and the brain.mgz file output from FreeSurfer were used as input to the trained deep learning model as described in this paper:

Yin, C., Imms, P., Cheng, M., Amgalan, A., Chowdhury, N. F., Massett, R. J., Chaudhari, N. N., Chen, X., Thompson, P. M., Bogdan, P., Irimia, A., & Alzheimer's Disease Neuroimaging Initiative (2023). Anatomically interpretable deep learning of brain age captures domain-specific cognitive impairment. *Proceedings of the National Academy of Sciences of the United States of America*, *120*(2), e2214634120. https://doi.org/10.1073/pnas.2214634120 **PMID**: 36595679

GitHub link: https://github.com/irimia-laboratory/USC_BA_estimator

DIFFUSION-WEIGHTED IMAGING (DWI)-BASED MEASUREMENTS

Scanning parameters: A Stejskal-Tanner [J. Chem. Phys. 42, 288 (1965)] diffusion prepared spin echo EPI sequence was used with the following parameters: 74-75 x 2 mm sagittal slices, within plane field of view = 256mm x 256 mm, acquisition matrix 128 x 128 (readout R/L), partial Fourier encoding 62.5% and ASSET (SENSE) x 2. Additional parameters TR = 8575 ms; TE = 76.6 ms. Six reference scans (b=0 s/mm^2) and three concentric shells (b=500 s/mm^2, b=800 s/mm^2, and b=2000 s/mm^2) were acquired with 9, 18, and 36 uniformly spread directions respectively.

Image processing: Preprocessing of the multi-shell diffusion weighted imaging (DWI) data was performed using the DESIGNER (Ades-Aron et al., 2018) pipeline which included the removal or mitigation of artifacts such as thermal noise, Gibb's ringing, distortion due to eddy currents, EPI distortion due to field inhomogeneities, and B1 and Rician bias correction using tools in FSL (Jenkinson et al., 2012), ANTs (Avants et al., 2009; Avants et al., 2011), and MRtrix3 (Tournier et al., 2019). The curated DWI data were used to estimate the diffusion kurtosis imaging (DKI) (Fieremans et al., 2011)

model which was then used to extract the diffusion tensor imaging (DTI) (Alexander et al., 2011; Jones & Leemans, 2011; Le Bihan et al., 2001) as well as the white matter tract integrity (WMTI) (Fieremans et al., 2013; Jelescu et al., 2015) metrics. The DKI and WMTI measures were smoothed to address spatial discontinuities ('black holes') and underestimation bias in the kurtosis estimates. Similar to the tissue specific, smoothing-compensated (T-SPOON, Lee et al., 2009) approach used in DTI analysis, spatially adaptive smoothing was performed using a mask where mean kurtosis > 0.3. The DWI data were also used to fit the multi-tissue neurite orientation dispersion and density imaging (NODDI) (Adluru et al., 2014; Fick et al., 2019; Guerrero et al., 2019; H. Zhang et al., 2012) model and derive the corresponding metrics (see below for brief summary of the different measures from these models).

These measures were spatially normalized to an iteratively estimated population specific coordinate system using ANTs. The population template was using a multi-variate approach using FA (Fractional Anisotropy) and MD (Mean Diffusivity) measures. The JHU (FSL v6.0.4) and IIT (v5.0) (Qi & Arfanakis, 2021) atlases were warped to the population specific coordinate system and subsequently to the participant specific (native) coordinate system. Median values for the 48 JHU binary regions and weighted median (Cormen et al., 2022; Guerrero-Gonzalez et al., 2022; Surgent et al., 2022) values were computed for the 42 IIT probabilistic regions, both in the native coordinate system. Similarly, the Harvard-Oxford subcortical atlas (Frazier et al., 2005) regions with a 50% probability threshold from FSL v6.0.4 were warped to the population specific coordinate system and subsequently to the participant specific (native) coordinate system. Median values were then computed in the native coordinate system.

Global summary measures in the brain were also computed using weighted median for each of the major tissue types (white matter, gray matter, and cerebrospinal fluid) generated in the native coordinate system using the FMRIB's Automated Segmentation Tool (FAST) (Zhang et al., 2001) in FSL.

Below is a brief summary of the different measures from these models.

DTI measures (Alexander et al., 2011) - The following metrics are widely used:

- Fractional anisotropy (FA) - **[C5WF…]** is the normalized standard deviation of the eigenvalues of the DTI. It is very sensitive to changes in white matter microstructure, but not very specific, as it can be influenced by changes in neurite density and dispersion among other factors. Lower FA is associated with aging.
- Mean diffusivity (MD) - **[C5WM…]** is the average diffusivity across the three principal directions. It is affected by both membrane density and fluid viscosity. Higher values of MD are associated with aging.
- Radial diffusivity (RD) - **[C5WR…]** measures diffusivity perpendicular to the axons. Higher values are associated with demyelination.
- Axial diffusivity (AD) - **[C5WA…]** measures diffusivity along the axons. AD is influenced by several factors, including axonal density, axonal diameter, and myelination, as well as the degree of water restriction along the fiber tract. Higher values of AD are associated with aging.

DKI measures (Jensen et al., 2005) - With higher diffusion weighting (b-values higher than 1000 s/mm2), non-gaussian diffusion effects arise. Kurtosis represents the deviation of diffusion from a normal displacement distribution and is a measure of the heterogeneity of the diffusion environment (Jensen & Helpern, 2010). DKI provides measures such as

- Mean kurtosis (MK) - **[C5WN…]** is the mean of the excess kurtosis for all diffusion directions, indexes the complexity of tissue microstructure. It represents a direction-independent index of diffusional heterogeneity (Coutu et al., 2014).
- Radial kurtosis (RK) - **[C5WS…]** is the diffusional kurtosis averaged over its perpendicular directions.
- Axial kurtosis (AK) - **[C5WB…]** is the diffusional kurtosis in the principal diffusion direction

These measures show strong age-dependence, declining with old age with regional differences (Das et al., 2017) and have been shown to discriminate individuals with mild cognitive impairment from controls (Falangola et al., 2013).

WMTI measures (Fieremans et al., 2013; Fieremans et al., 2011) - DTI and DKI are both model-independent metrics that are not necessarily specific to biological changes. To enable interpretation, WMTI uses a two-compartment model (intra-axonal and extra-axonal space, IAS and EAS) yielding the following metrics:

- Axonal water fraction (AWF) - **[C5WX…]** is a marker of axonal density and lower values suggest reduction in axons potentially due to Wallerian degeneration after distal cortical atrophy.
- Intra-axonal diffusivity (ias_Da) - **[C5WI…]** represents intrinsic diffusivity within axons, may be a marker of axonal injury.
- Extra-axonal radial diffusivity (eas_de_perp) - **[C5WP…]** is a marker for changes in diffusion transverse to fibers due to myelin breakdown.
- Extra-axonal tortuosity (eas_tort) - **[C5WT…]** is an indirect measure of myelinated axonal fraction/myelin density; higher values for lower EAS volume fraction

NODDI measures (Adluru et al., 2014; Fick et al., 2019; Guerrero et al., 2019; H. Zhang et al., 2012) - The NODDI approach uses a multi-compartment model and allows estimation of the following metrics:

- Neurite density index (NDI) - **[C5WD…]** is an indicator of myelination and axonal integrity (Nazeri et al., 2020). Lower NDI is suggestive of demyelinating processes, potentially including neuronal loss.
- Orientation dispersion index (ODI) - **[C5WV…]** indicates the spread of neurites (dendrites and axons). Higher ODI in white matter may reflect axonal disorganization with aging (Billiet et al., 2015).
- Fraction of isotropic diffusion (FISO or CSF) - **[C5WC…]** is indicative of free water or cerebrospinal fluid (CSF) content. Higher values are associated with aging (Billiet et al., 2015).

For 153 participants, median (or weighted median for the IIT v5.0 regions) estimates of DWI-based metrics are provided for

- global summary of the major tissue types (white matter, gray matter, and cerebrospinal fluid) **[C5W_G…]**
- tract-specific measures extracted using multiple atlases:
    - JHU ICBM-DTI-81 **[C5W_ _J…]** (http://cmrm.med.jhmi.edu/; Hua et al., 2008; Mori et al., 2008; Wakana et al., 2007) with FSL v6.0.4 (https://fsl.fmrib.ox.ac.uk/fsl/fslwiki/Atlases)

    - IIT v5.0 **[C5W_ _K…]** (https://www5.iit.edu/~mri/IITHumanBrainAtlas.html; Qi & Arfanakis, 2021; S. Zhang & Arfanakis, 2018) white-matter atlases
- the Harvard-Oxford Subcortical Atlas **[C5W_ _H…]** (Makris et al., 2006; Frazier et al., 2005; Desikan et al., 2006; Goldstein et al., 2007) regions with a 50% probability threshold with FSL v6.0.4

VARIABLE NAMING

Partial variable names listed below. For more detailed information on variable names see atlas tables below or *M3_P5_VARIABLE_NAMES_20260206*.

Scan type:

[C5E…]: T1-weighted (Extracted structural measures)

[C5W…]: Diffusion-weighted (Extracted diffusion weighted imaging measures)

Measurement type:

[C5ET…]: Cortical Thickness (mm)

[C5EC…]: Cortical Curvature (mm)

[C5EA…]: Cortical Surface Area (mm^2)

[C5EV…]: Cortical Volume (mm^3)

[C5ES…]: Subcortical Volume (mm^3)

[C5WF…]: Fractional Anisotropy (FA)

[C5WM…]: Mean Diffusivity (MD)

[C5WR…]: Radial Diffusivity (RD)

[C5WA…]: Axial Diffusivity (AD)

[C5WN…]: Mean Kurtosis (MK)

[C5WS…]: Radial Kurtosis (RK)

[C5WB…]: Axial Kurtosis (AK)

[C5WX…]: Axonal Water Fraction (AWF)

[C5WI…]: Intra-axonal diffusivity (ias_Da)

[C5WP…]: Extra-axonal radial diffusivity (eas_de_perp)

[C5WT…]: Extra-axonal tortuosity (eas_tort)

[C5WD…]: Neurite density index (NDI)

[C5WV…]: Orientation dispersion index (ODI)

[C5WC…]: Fraction of isotropic diffusion (FISO or CSF)

Hemisphere: Note that '_' represents any one of the measurement variables listed above.

[C5_ _G…]: Measurement is global (encompasses entire brain)

[C5_ _L…]: Measurement is specific to left hemisphere

[C5_ _R…]: Measurement is specific to right hemisphere

[C5_ _N…]: Not applicable; measurement is bilateral

Atlas: Note that '_' represents any one of the measurement and hemisphere variables listed above.

[C5E_ _D…]: Measurement calculated using Destrieux brain atlas (Fischl et al., 2004b).

[C5E_ _K…]: Measurement calculated using Desikan-Killiany brain atlas (Desikan et al., 2006).

[C5E_ _T…]: Measurement calculated using Desikan-Killiany-Tourville brain atlas (Klein & Tourville, 2012).

[C5E_ _A…]: Measurement calculated using FreeSurfer aseg subcortical brain atlas (Fischl et al., 2002) or Hippocampal Subfield (Iglesias et al., 2015) and Amygdala Nuclei (Saygin & Kliemann et al., 2017) module.

[C5W_ _H…]: Measurement calculated using Harvard-Oxford subcortical structural atlas (Makris et al., 2006; Frazier et al., 2005; Desikan et al., 2006; Goldstein et al., 2007).

[C5W_ _K…]: Measurement calculated using IIT v5.0 white matter atlas (Qi & Arfanakis, 2021; S. Zhang & Arfanakis, 2018).

[C5W_ _J…]: Measurement calculated using JHU white matter atlas (Hua et al., 2008; Mori et al., 2008; and Wakana et al., 2007).

Brain-Based Aging Algorithm:

[C5EB]: Brain-Predicted Age (yrs) estimated using Cole brainageR v1.0 - https://github.com/james-cole/brainageR/tree/1.0

[C5EBC]: Brain-Predicted Age (yrs) estimated using Cole brainageR v2.0 - https://github.com/james-cole/brainageR/tree/2.0

[C5EBT]: Brain-Predicted Age (yrs) estimated using two-stage-age-network (TSAN) model from PMID: 34086565 - https://github.com/Milan-BUAA/TSAN-brain-age-estimation

[C5EBP]: Brain-Predicted Age (yrs) estimated using 3D-CNN model from PMID: 36595679 - https://github.com/irimia-laboratory/USC_BA_estimator

[C5EBD]: DunedinPACNI Dunedin Pace of Aging Calculated from NeuroImaging from PMID: 40595015 - https://github.com/etw11/DunedinPACNI

ATLAS/MODULE TABLES

DESTRIEUX CORTICAL ATLAS

VARIABLE LABEL (FROM SPSS FILE)	FULL NAME OF PARCELLATION	VARIABLE NAME
G_and_S_frontomargin	Fronto-marginal gyrus (of Wernicke) and sulcus	C5E_ _D01
G_and_S_occipital_inf	Inferior occipital gyrus (O3) and sulcus	C5E_ _D02
G_and_S_paracentral	Paracentral lobule and sulcus	C5E_ _D03
G_and_S_subcentral	Subcentral gyrus (central operculum) and sulci	C5E_ _D04
G_and_S_transv_frontopol	Transverse frontopolar gyri and sulci	C5E_ _D05
G_and_S_cingul-Ant	Anterior part of the cingulate gyrus and sulcus (ACC)	C5E_ _D06
G_and_S_cingul-Mid-Ant	Middle-anterior part of the cingulate gyrus and sulcus (aMCC)	C5E_ _D07
G_and_S_cingul-Mid-Post	Middle-posterior part of the cingulate gyrus and sulcus (pMCC)	C5E_ _D08
G_cingul-Post-dorsal	Posterior-dorsal part of the cingulate gyrus (dPCC)	C5E_ _D09
G_cingul-Post-ventral	Posterior-ventral part of the cingulate gyrus (vPCC, isthmus of the cingulate gyrus)	C5E_ _D10
G_cuneus	Cuneus (O6)	C5E_ _D11
G_front_inf-Opercular	Opercular part of the inferior frontal gyrus	C5E_ _D12
G_front_inf-Orbital	Orbital part of the inferior frontal gyrus	C5E_ _D13
G_front_inf-Triangul	Triangular part of the inferior frontal gyrus	C5E_ _D14
G_front_middle	Middle frontal gyrus (F2)	C5E_ _D15
G_front_sup	Superior frontal gyrus (F1)	C5E_ _D16
G_Ins_lg_and_S_cent_ins	Long insular gyrus and central sulcus of the insula	C5E_ _D17
G_insular_short	Short insular gyri	C5E_ _D18
G_occipital_middle	Middle occipital gyrus (O2, lateral occipital gyrus)	C5E_ _D19
G_occipital_sup	Superior occipital gyrus (O1)	C5E_ _D20
G_oc-temp_lat-fusifor	Lateral occipito-temporal gyrus (fusiform gyrus, O4-T4)	C5E_ _D21
G_oc-temp_med-Lingual	Lingual gyrus, ligual part of the medial occipito-temporal gyrus, (O5)	C5E_ _D22
G_oc-temp_med-Parahip	Parahippocampal gyrus, parahippocampal part of the medial occipito-temporal gyrus, (T5)	C5E_ _D23
G_orbital	Orbital gyri	C5E_ _D24
G_pariet_inf-Angular	Angular gyrus	C5E_ _D25
G_pariet_inf-Supramar	Supramarginal gyrus	C5E_ _D26
G_parietal_sup	Superior parietal lobule (lateral part of P1)	C5E_ _D27
G_postcentral	Postcentral gyrus	C5E_ _D28
G_precentral	Precentral gyrus	C5E_ _D29
G_precuneus	Precuneus (medial part of P1)	C5E_ _D30
G_rectus	Straight gyrus, Gyrus rectus	C5E_ _D31
G_subcallosal	Subcallosal area, subcallosal gyrus	C5E_ _D32
G_temp_sup-G_T_transv	Anterior transverse temporal gyrus (of Heschl)	C5E_ _D33
G_temp_sup-Lateral	Lateral aspect of the superior temporal gyrus	C5E_ _D34
G_temp_sup-Plan_polar	Planum polare of the superior temporal gyrus	C5E_ _D35

G_temp_sup-Plan_tempo	Planum temporale or temporal plane of the superior temporal gyrus	C5E_ _D36
G_temporal_inf	Inferior temporal gyrus (T3)	C5E_ _D37
G_temporal_middle	Middle temporal gyrus (T2)	C5E_ _D38
Lat_Fis-ant-Horizon	Horizontal ramus of the anterior segment of the lateral sulcus (or fissure)	C5E_ _D39
Lat_Fis-ant-Vertical	Vertical ramus of the anterior segment of the lateral sulcus (or fissure)	C5E_ _D40
Lat_Fis-post	Posterior ramus (or segment) of the lateral sulcus (or fissure)	C5E_ _D41
Pole_occipital	Occipital pole	C5E_ _D42
Pole_temporal	Temporal pole	C5E_ _D43
S_calcarine	Calcarine sulcus	C5E_ _D44
S_central	Central sulcus (Rolando's fissure)	C5E_ _D45
S_cingul-Marginalis	Marginal branch (or part) of the cingulate sulcus	C5E_ _D46
S_circular_insula_ant	Anterior segment of the circular sulcus of the insula	C5E_ _D47
S_circular_insula_inf	Inferior segment of the circular sulcus of the insula	C5E_ _D48
S_circular_insula_sup	Superior segment of the circular sulcus of the insula	C5E_ _D49
S_collat_transv_ant	Anterior transverse collateral sulcus	C5E_ _D50
S_collat_transv_post	Posterior transverse collateral sulcus	C5E_ _D51
S_front_inf	Inferior frontal sulcus	C5E_ _D52
S_front_middle	Middle frontal sulcus	C5E_ _D53
S_front_sup	Superior frontal sulcus	C5E_ _D54
S_interm_prim-Jensen	Sulcus intermedius primus (of Jensen)	C5E_ _D55
S_intrapariet_and_P_trans	Intraparietal sulcus (interparietal sulcus) and transverse parietal sulci	C5E_ _D56
S_oc_middle_and_Lunatus	Middle occipital sulcus and lunatus sulcus	C5E_ _D57
S_oc_sup_and_transversal	Superior occipital sulcus and transverse occipital sulcus	C5E_ _D58
S_occipital_ant	Anterior occipital sulcus and preoccipital notch (temporo-occipital incisure)	C5E_ _D59
S_oc-temp_lat	Lateral occipito-temporal sulcus	C5E_ _D60
S_oc-temp_med_and_Lingual	Medial occipito-temporal sulcus (collateral sulcus) and lingual sulcus	C5E_ _D61
S_orbital_lateral	Lateral orbital sulcus	C5E_ _D62
S_orbital_med-olfact	Medial orbital sulcus (olfactory sulcus)	C5E_ _D63
S_orbital-H_Shaped	Orbital sulci (H-shaped sulci)	C5E_ _D64
S_parieto_occipital	Parieto-occipital sulcus (or fissure)	C5E_ _D65
S_pericallosal	Pericallosal sulcus (S of corpus callosum)	C5E_ _D66
S_postcentral	Postcentral sulcus	C5E_ _D67
S_precentral-inf-part	Inferior part of the precentral sulcus	C5E_ _D68
S_precentral-sup-part	Superior part of the precentral sulcus	C5E_ _D69
S_suborbital	Suborbital sulcus (sulcus rostrales, supraorbital sulcus)	C5E_ _D70
S_subparietal	Subparietal sulcus	C5E_ _D71
S_temporal_inf	Inferior temporal sulcus	C5E_ _D72
S_temporal_sup	Superior temporal sulcus (parallel sulcus)	C5E_ _D73
S_temporal_transverse	Transverse temporal sulcus	C5E_ _D74

DESIKAN-KILLIANY CORTICAL ATLAS

VARIABLE LABEL (FROM SPSS FILE)	FULL NAME OF PARCELLATION	VARIABLE NAME
bankssts	Banks superior temporal sulcus	C5E_ _K01
caudalanteriorcingulate	Caudal anterior-cingulate cortex	C5E_ _K02
caudalmiddlefrontal	Caudal middle frontal gyrus	C5E_ _K03
cuneus	Cuneus cortex	C5E_ _K04
entorhinal	Entorhinal cortex	C5E_ _K05
fusiform	Fusiform gyrus	C5E_ _K06
inferiorparietal	Inferior parietal cortex	C5E_ _K07
inferiortemporal	Inferior temporal gyrus	C5E_ _K08
isthmuscingulate	Isthmus– cingulate cortex	C5E_ _K09
lateraloccipital	Lateral occipital cortex	C5E_ _K10
lateralorbitofrontal	Lateral orbital frontal cortex	C5E_ _K11
lingual	Lingual gyrus	C5E_ _K12
medialorbitofrontal	Medial orbital frontal cortex	C5E_ _K13
middletemporal	Middle temporal gyrus	C5E_ _K14
parahippocampal	Parahippocampal gyrus	C5E_ _K15
paracentral	Paracentral lobule	C5E_ _K16
parsopercularis	Pars opercularis	C5E_ _K17
parsorbitalis	Pars orbitalis	C5E_ _K18
parstriangularis	Pars triangularis	C5E_ _K19
pericalcarine	Pericalcarine cortex	C5E_ _K20
postcentral	Postcentral gyrus	C5E_ _K21
posteriorcingulate	Posterior-cingulate cortex	C5E_ _K22
precentral	Precentral gyrus	C5E_ _K23
precuneus	Precuneus cortex	C5E_ _K24
rostralanteriorcingulate	Rostral anterior cingulate cortex	C5E_ _K25
rostralmiddlefrontal	Rostral middle frontal gyrus	C5E_ _K26
superiorfrontal	Superior frontal gyrus	C5E_ _K27
superiorparietal	Superior parietal cortex	C5E_ _K28
superiortemporal	Superior temporal gyrus	C5E_ _K29
supramarginal	Supramarginal gyrus	C5E_ _K30
frontalpole	Frontal pole	C5E_ _K31
temporalpole	Temporal pole	C5E_ _K32
transversetemporal	Transverse temporal cortex	C5E_ _K33
insula	Insula	C5E_ _K34

DESIKAN-KILLIANY-TOURVILLE – DKT - CORTICAL ATLAS

VARIABLE LABEL (FROM SPSS FILE)	FULL NAME OF PARCELLATION	VARIABLE NAME
caudalanteriorcingulate	Caudal anterior-cingulate cortex	C5E_ _T01
caudalmiddlefrontal	Caudal middle frontal gyrus	C5E_ _T02
cuneus	Cuneus cortex	C5E_ _T03

entorhinal	Entorhinal cortex	C5E_ _T04
fusiform	Fusiform gyrus	C5E_ _T05
inferiorparietal	Inferior parietal cortex	C5E_ _T06
inferiortemporal	Inferior temporal gyrus	C5E_ _T07
isthmuscingulate	Isthmus– cingulate cortex	C5E_ _T08
lateraloccipital	Lateral occipital cortex	C5E_ _T09
lateralorbitofrontal	Lateral orbital frontal cortex	C5E_ _T10
lingual	Lingual gyrus	C5E_ _T11
medialorbitofrontal	Medial orbital frontal cortex	C5E_ _T12
middletemporal	Middle temporal gyrus	C5E_ _T13
parahippocampal	Parahippocampal gyrus	C5E_ _T14
paracentral	Paracentral lobule	C5E_ _T15
parsopercularis	Pars opercularis	C5E_ _T16
parsorbitalis	Pars orbitalis	C5E_ _T17
parstriangularis	Pars triangularis	C5E_ _T18
pericalcarine	Pericalcarine cortex	C5E_ _T19
postcentral	Postcentral gyrus	C5E_ _T20
posteriorcingulate	Posterior-cingulate cortex	C5E_ _T21
precentral	Precentral gyrus	C5E_ _T22
precuneus	Precuneus cortex	C5E_ _T23
rostralanteriorcingulate	Rostral anterior cingulate cortex	C5E_ _T24
rostralmiddlefrontal	Rostral middle frontal gyrus	C5E_ _T25
superiorfrontal	Superior frontal gyrus	C5E_ _T26
superiorparietal	Superior parietal cortex	C5E_ _T27
superiortemporal	Superior temporal gyrus	C5E_ _T28
supramarginal	Supramarginal gyrus	C5E_ _T29
transversetemporal	Transverse temporal cortex	C5E_ _T30
insula	Insula	C5E_ _T31

ASEG SUBCORTICAL ATLAS

VARIABLE LABEL (FROM SPSS FILE)	FULL NAME OF PARCELLATION	VARIABLE NAME
Lateral-Ventricle	Lateral Ventricle	C5ES_A09
Inf-Lat-Vent	Inferior Lateral Ventricle	C5ES_A08
Cerebellum-White-Matter	Cerebellum White Matter	C5ES_A05
Cerebellum-Cortex	Cerebellum Cortex	C5ES_A04
Thalamus-Proper	Thalamus	C5ES_A12
Caudate	Caudate	C5ES_A03
Putamen	Putamen	C5ES_A11
Pallidum	Pallidum	C5ES_A10
Hippocampus	Hippocampus	C5ES_A07
Amygdala	Amygdala	C5ES_A02
Accumbens-area	Accumbens Area	C5ES_A01
VentralDC	Ventral Diencephalon	C5ES_A13

vessel	vessel (non-specific)	C5ES_A14
3rd-Ventricle	Third Ventricle	C5ESNA01
4th-Ventricle	Fourth Ventricle	C5ESNA02
Brain-Stem	Brain Stem	C5ESNA03
CSF	Cerebrospinal Fluid	C5ESNA15
choroid-plexus	Choroid Plexus	C5ES_A06
CortexVol	Cortical Gray Matter Volume	C5ES_A15 OR C5ESNA13
CerebralWhiteMatterVol*	Cerebral White Matter Volume*	C5ES_A16 OR C5ESNA14
SurfaceHoles	Number of defect holes in surfaces prior to fixing	C5ES_A17 OR C5ESNA24
BrainSegVol	Brain Segmentation Volume	C5ESNA04
BrainSegVol-to-eTIV	Ratio of BrainSegVol to estimated Total Intracranial Volume	C5ESNA05
BrainSegVolNotVent	Brain Segmentation Volume Without Ventricles	C5ESNA06
BrainSegVolNotVentSurf	Brain Segmentation Volume Without Ventricles from Surf	C5ESNA07
CC_Anterior	Anterior Corpus Callosum	C5ESNA08
CC_Central	Central Corpus Callosum	C5ESNA09
CC_Mid_Anterior	Mid-Anterior Corpus Callosum	C5ESNA10
CC_Mid_Posterior	Mid-Posterior Corpus Callosum	C5ESNA11
CC_Posterior	Posterior Corpus Callosum	C5ESNA12
EstimatedTotalIntraCranialVol	Estimated Total Intracranial Volume	C5ESNA16
MaskVol	Mask Volume	C5ESNA17
MaskVol-to-eTIV	Ratio of MaskVol to estimated Total Intracranial Volume	C5ESNA18
Optic-Chiasm	Optic Chiasm	C5ESNA19
SubCortGrayVol	Subcortical Gray Matter Volume	C5ESNA20
SupraTentorialVol	Supratentorial Volume	C5ESNA21
SupraTentorialVolNotVent	Supratentorial Volume Without Ventricles	C5ESNA22
SupraTentorialVolNotVentVox	Supratentorial Volume Voxel Count	C5ESNA23
TotalGrayVol	Total Gray Matter Volume	C5ESNA25

*FreeSurfer creators renamed variable from “CorticalWhiteMatterVol” in FreeSurfer v5.3.0 (used for MR1) to “CerebralWhiteMatterVol” in FreeSurfer v6.0.0 (used for M3). Same variable meaning, only change in naming convention.

AMYGDALA ATLAS

VARIABLE LABEL (FROM SPSS FILE)	FULL NAME OF PARCELLATION	VARIABLE NAME
Lateral-nucleus	Lateral nucleus	C5ES_A18
Basal-nucleus	Basal nucleus	C5ES_A19
Accessory-basal-nucleus	Accessory basal nucleus	C5ES_A20
Anterior-amygdaloid-area-AAA	Anterior amygdaloid area	C5ES_A21
Central-nucleus	Central nucleus	C5ES_A22
Medial-nucleus	Medial nucleus	C5ES_A23

Cortical-nucleus	Cortical nucleus	C5ES_A24
Corticoamygdaloid-transitio	Corticoamygdaloid transition area	C5ES_A25
Paralaminar-nucleus	Paralaminar nucleus	C5ES_A26
Whole_amygdala	Amygdala	C5ES_A27

HIPPOCAMPUS ATLAS

VARIABLE LABEL (FROM SPSS FILE)	FULL NAME OF PARCELLATION	VARIABLE NAME
Hippocampal_tail	Hippocampal tail	C5ES_A28
Subiculum-body	Subiculum (body)	C5ES_A29
CA1-body	Cornu ammonis 1 (body)	C5ES_A30
Subiculum-head	Subiculum (head)	C5ES_A31
Hippocampal-fissure	Hippocampal fissure	C5ES_A32
Presubiculum-head	Presubiculum (head)	C5ES_A33
CA1-head	Cornu ammonis 1 (head)	C5ES_A34
Presubiculum-body	Presubiculum (body)	C5ES_A35
Parasubiculum	Parasubiculum	C5ES_A36
Molecular_layer_HP-head	Molecular layer (head)	C5ES_A37
Molecular_layer_HP-body	Molecular layer (body)	C5ES_A38
GC-ML-DG-head	Granule cell (GC) and molecular layer (ML) of the dentate gyrus (DG) (head)	C5ES_A39
CA3-body	Cornu ammonis 3 (body)	C5ES_A40
GC-ML-DG-body	Granule cell (GC) and molecular layer (ML) of the dentate gyrus (DG) (body)	C5ES_A41
CA4-head	Cornu ammonis 4 (head)	C5ES_A42
CA4-body	Cornu ammonis 4 (body)	C5ES_A43
Fimbria	Fimbria	C5ES_A44
CA3-head	Cornu ammonis 3 (head)	C5ES_A45
HATA	Hippocampus-amygdala-transition-area	C5ES_A46
Whole_hippocampal_body	Hippocampal body	C5ES_A47
Whole_hippocampal_head	Hippocampal head	C5ES_A48
Whole_hippocampus	Hippocampus	C5ES_A49

JHU WHITE MATTER BUNDLES ATLAS

VARIABLE LABEL (FROM SPSS FILE)	FULL NAME OF PARCELLATION	VARIABLE NAME
Anterior_corona_radiata	Anterior corona radiata	C5W_ _J01
Anterior_limb_of_internal_capsule	Anterior limb of internal capsule	C5W_ _J02
Cerebral_peduncle	Cerebral peduncle	C5W_ _J03
Cingulum_(cingulate_gyrus)	Cingulum (cingulate gyrus)	C5W_ _J04
Cingulum_(hippocampus)	Cingulum (hippocampus)	C5W_ _J05
Corticospinal_tract	Corticospinal tract	C5W_ _J06

External_capsule	External capsule	C5W_ _J07
Fornix_(cres)_-_Stria_terminalis_ (can_not_be_resolved_with_current_resolution)	Fornix (cres) / Stria terminalis (cannot be resolved with current resolution)	C5W_ _J08
Inferior_cerebellar_peduncle	Inferior cerebellar peduncle	C5W_ _J09
Medial_lemniscus	Medial lemniscus	C5W_ _J10
Posterior_corona_radiata	Posterior corona radiata	C5W_ _J11
Posterior_limb_of_internal_capsule	Posterior limb of internal capsule	C5W_ _J12
Posterior_thalamic_radiation_ (include_optic_radiation)	Posterior thalamic radiation (includes optic radiation)	C5W_ _J13
Retrolenticular_part_of_internal_capsule	Retrolenticular part of internal capsule	C5W_ _J14
Sagittal_stratum_(include_inferior_longitidinal_ fasciculus_and_inferior_fronto-occipital_fasciculus)	Sagittal stratum (includes inferior longitudinal fasciculus and inferior fronto-occipital fasciculus)	C5W_ _J15
Superior_cerebellar_peduncle	Superior cerebellar peduncle	C5W_ _J16
Superior_corona_radiata	Superior corona radiata	C5W_ _J17
Superior_fronto-occipital_fasciculus_ (could_be_a_part_of_anterior_internal_capsule)	Superior fronto-occipital fasciculus (could be a part of anterior internal capsule)	C5W_ _J18
Superior_longitudinal_fasciculus	Superior longitudinal fasciculus	C5W_ _J19
Tapetum	Tapetum	C5W_ _J20
Uncinate_fasciculus	Uncinate fasciculus	C5W_ _J21
Body_of_corpus_callosum	Body of corpus callosum	C5W_NJ01
Fornix_(column_and_body_of_fornix)	Fornix (column and body of fornix)	C5W_NJ02
Genu_of_corpus_callosum	Genu of corpus callosum	C5W_NJ03
Middle_cerebellar_peduncle	Middle cerebellar peduncle	C5W_NJ04
Pontine_crossing_tract_(a_part_of_MCP)	Pontine crossing tract (a part of MCP)	C5W_NJ05
Splenium_of_corpus_callosum	Splenium of corpus callosum	C5W_NJ06

IIT V5.0 WHITE MATTER BUNDLES ATLAS

VARIABLE LABEL (FROM SPSS FILE)	FULL NAME OF PARCELLATION	VARIABLE NAME
Anterior_commissure	Anterior commissure	C5W_NK01
Arcuate_fasciculus	Arcuate fasciculus	C5W_ _K01
Frontal_aslant_tract	Frontal aslant tract	C5W_ _K02
Cingulum	Cingulum	C5W_ _K03
Corpus_callosum	Corpus callosum	C5W_NK02
Forceps_major	Forceps major	C5W_NK03
Forceps_minor	Forceps minor	C5W_NK04
Middle_corpus_callosum	Middle corpus callosum	C5W_NK05
Corticospinal_tract	Corticospinal tract	C5W_ _K04
Fornix	Fornix	C5W_NK06
Frontopontine	Frontopontine	C5W_ _K05
Inferior_cerebellar_peduncle	Inferior cerebellar peduncle	C5W_ _K06
Inferior_frontooccipital_fasciculus	Inferior frontooccipital fasciculus	C5W_ _K07
Inferior_longitudinal_fasciculus	Inferior longitudinal fasciculus	C5W_ _K08
Middle_cerebellar_peduncle	Middle cerebellar peduncle	C5W_NK07

Middle_longitudinal_fasciculus	Middle longitudinal fasciculus	C5W_ _K09
Medial_lemniscus	Medial lemniscus	C5W_ _K10
Occipitopontine_tract	Occipitopontine tract	C5W_ _K11
Optic_radiation	Optic radiation	C5W_ _K12
Parietopontine_tract	Parietopontine tract	C5W_ _K13
Superior_cerebellar_peduncle	Superior cerebellar peduncle	C5W_NK08
Superior_longitudinal_fasciculus	Superior longitudinal fasciculus	C5W_ _K14
Spinothalamic_tract	Spinothalamic tract	C5W_ _K15
Uncinate_fasciculus	Uncinate fasciculus	C5W_ _K16
Vertical_occipital_fasciculus	Vertical occipital fasciculus	C5W_ _K17

HARVARD-OXFORD SUBCORTICAL STRUCTURAL ATLAS

VARIABLE LABEL (FROM SPSS FILE)	FULL NAME OF PARCELLATION	VARIABLE NAME
Amygdala	Amygdala	C5W_ _H01
Caudate	Caudate	C5W_ _H02
Cerebral Cortex	Cerebral Cortex	C5W_ _H03
Hippocampus	Hippocampus	C5W_ _H04
Accumbens	Nucleus Accumbens	C5W_ _H05
Pallidum	Pallidum	C5W_ _H06
Putamen	Putamen	C5W_ _H07
Thalamus	Thalamus	C5W_ _H08
Cerebral White Matter	Cerebral White Matter	C5W_ _H09

REFERENCES

Ades-Aron, B., Veraart, J., Kochunov, P., McGuire, S., Sherman, P., Kellner, E., Novikov, D. S., & Fieremans, E. (2018). Evaluation of the accuracy and precision of the diffusion parameter EStImation with Gibbs and NoisE removal pipeline. *NeuroImage*, *183*, 532–543. https://doi.org/10.1016/j.neuroimage.2018.07.066

Adluru, G., Gur, Y., Anderson, J. S., Richards, L. G., Adluru, N., & DiBella, E. V. (2014). Assessment of white matter microstructure in stroke patients using NODDI. *Annual International Conference of the IEEE Engineering in Medicine and Biology Society. IEEE Engineering in Medicine and Biology Society. Annual International Conference*, *2014*, 742–745. https://doi.org/10.1109/EMBC.2014.6943697

Alexander, A. L., Hurley, S. A., Samsonov, A. A., Adluru, N., Hosseinbor, A. P., Mossahebi, P., Tromp, doP. M., Zakszewski, E., & Field, A. S. (2011). Characterization of cerebral white matter properties using quantitative magnetic resonance imaging stains. *Brain connectivity*, *1*(6), 423–446. https://doi.org/10.1089/brain.2011.0071

Avants, B. B., Tustison, N. J., Song, G. (2009). Advanced Normalization Tools (ANTS). *Insight Journal*. https://doi.org/10.54294/uvnhin

Avants, B. B., Tustison, N. J., Song, G., Cook, P. A., Klein, A., & Gee, J. C. (2011). A reproducible evaluation of ANTs similarity metric performance in brain image registration. *NeuroImage*, *54*(3), 2033–2044. https://doi.org/10.1016/j.neuroimage.2010.09.025

Billiet, T., Vandenbulcke, M., Mädler, B., Peeters, R., Dhollander, T., Zhang, H., Deprez, S., Van den Bergh, B. R., Sunaert, S., & Emsell, L. (2015). Age-related microstructural differences quantified using myelin water imaging and advanced diffusion MRI. *Neurobiology of aging*, *36*(6), 2107–2121. https://doi.org/10.1016/j.neurobiolaging.2015.02.029

Cheng, J., Liu, Z., Guan, H., Wu, Z., Zhu, H., Jiang, J., … Liu, T. (2021). Brain Age Estimation From MRI Using Cascade Networks With Ranking Loss. *IEEE Transactions on Medical Imaging*, *40*(12), 3400–3412. doi: 10.1109/tmi.2021.3085948 PMID: 34086565

Cole JH, Leech R, Sharp DJ, for the Alzheimer's Disease Neuroimaging Initiative (2015). Prediction of brain age suggests accelerated atrophy after traumatic brain injury. *Ann Neurol 77(4)*: 571-581.

Cole JH, Poudel RPK, Tsagkrasoulis D, Caan MWA, Steves C, Spector TD et al. (2017). Predicting brain age with deep learning from raw imaging data results in a reliable and heritable biomarker. *NeuroImage*, *163C*: 115-124. doi: 10.1016/j.neuroimage.2017.07.059. Epub 2017 Jul 29. PMID: 28765056.

Cole JH, Ritchie SJ, Bastin ME, Valdes Hernandez MC, Munoz Maniega S, Royle N et al. (2018). Brain age predicts mortality. *Molecular psychiatry*, *23*: 1385-1392.

Cormen, T. H., Leiserson, C. E., Rivest, R. L., & Stein, C. (2022). *Introduction to algorithms* (4th ed.). MIT Press.

Coutu, J.-P., Chen, J. J., Rosas, H. D., & Salat, D. H. (2014). Non-Gaussian water diffusion in aging white matter. *Neurobiology of Aging*, *35*(6), 1412–1421. https://doi.org/10.1016/j.neurobiolaging.2013.12.001

Dale, A.M., Fischl, B., Sereno, M.I. (1999). Cortical surface-based analysis. I. Segmentation and surface reconstruction. *Neuroimage*, *9*, 179-194.

Dale, A.M., Sereno, M.I. (1993). Improved localization of cortical activity by combining EEG and MEG with MRI cortical surface reconstruction: a linear approach. *J Cogn Neurosci*, *5*, 162-176.

Das, S. K., Wang, J. L., Bing, L., Bhetuwal, A., & Yang, H. F. (2017). Regional Values of Diffusional Kurtosis Estimates in the Healthy Brain during Normal Aging. *Clinical Neuroradiology*, *27*(3), 283–298. https://doi.org/10.1007/s00062-015-0490-z

Desikan R.S., Ségonne F., Fischl B., Quinn B.T., Dickerson B.C., Blacker D., Buckner R.L., Dale A.M., Maguire R.P., Hyman B.T., Albert M.S., & Killiany R.J. (2006). An automated labeling system for subdividing the human cerebral cortex on MRI scans into gyral based regions of interest. *Neuroimage*, *31*(3), 968-980. https://doi.org/10.1016/j.neuroimage.2006.01.021

Falangola, M. F., Jensen, J. H., Tabesh, A., Hu, C., Deardorff, R. L., Babb, J. S., Ferris, S., & Helpern, J. A. (2013). Non-Gaussian diffusion MRI assessment of brain microstructure in mild cognitive impairment and Alzheimer's disease. *Magnetic Resonance Imaging*, *31*(6), 840–846. https://doi.org/10.1016/j.mri.2013.02.008

Fick, R. H. J., Wassermann, D., & Deriche, R. (2019). The Dmipy Toolbox: Diffusion MRI Multi-Compartment Modeling and Microstructure Recovery Made Easy. *Frontiers in neuroinformatics*, *13*, 64. https://doi.org/10.3389/fninf.2019.00064

Fieremans, E., Benitez, A., Jensen, J. H., Falangola, M. F., Tabesh, A., Deardorff, R. L., Spampinato, M. V., Babb, J. S., Novikov, D. S., Ferris, S. H., & Helpern, J. A. (2013). Novel white matter tract integrity metrics sensitive to Alzheimer disease progression. *AJNR. American journal of neuroradiology*, *34*(11), 2105–2112. https://doi.org/10.3174/ajnr.A3553

Fieremans, E., Jensen, J. H., & Helpern, J. A. (2011). White matter characterization with diffusional kurtosis imaging. *NeuroImage*, *58*(1), 177–188. https://doi.org/10.1016/j.neuroimage.2011.06.006

Fischl, B., Dale, A.M. (2000). Measuring the thickness of the human cerebral cortex from magnetic resonance images. *Proc Natl Acad Sci USA, 97,* 11050-11055.

Fischl, B., Liu, A., Dale, A.M. (2001). Automated manifold surgery: constructing geometrically accurate and topologically correct models of the human cerebral cortex. *IEEE Trans Med Imaging, 20*, 70-80.

Fischl B., Salat D.H., Busa E., Albert M., Dieterich M., Haselgrove C., van der Kouwe A., Killiany R., Kennedy D., Klaveness S., Montillo A., Makris N., Rosen B., & Anders M. Dale A.M. (2002). Whole brain segmentation: automated labeling of neuroanatomical structures in the human brain. *Neuron, 33*, 341-355.

Fischl, B., Salat, D.H., van der Kouwe, A.J., Makris, N., Segonne, F., Quinn, B.T., & Dale, A.M. (2004a). Sequence-independent segmentation of magnetic resonance images. *Neuroimage 23 Suppl 1*, S69-84.

Fischl, B., Sereno, M.I., Dale, A.M. (1999a). Cortical surface-based analysis. II: Inflation, flattening, and a surface-based coordinate system. *Neuroimage, 9*, 195-207.

Fischl, B., Sereno, M.I., Tootell, R.B., Dale, A.M. (1999b). High-resolution intersubject averaging and a coordinate system for the cortical surface. *Hum Brain Mapp, 8*, 272-284.

Fischl B., van der Kouwe A., Destrieux C., Halgren E., Ségonne F., Salat D.H., Busa E., Seidman L.J., Goldstein J., Kennedy D., Caviness V., Makris N., Rosen B., & Dale A.M. (2004b). Automatically parcellating the human cerebral cortex. *Cereb Cortex, 14(1)*, 11-22.

Frazier, J. A., Chiu, S., Breeze, J. L., Makris, N., Lange, N., Kennedy, D. N., Herbert, M. R., Bent, E. K., Koneru, V. K., Dieterich, M. E., Hodge, S. M., Rauch, S. L., Grant, P. E., Cohen, B. M., Seidman, L. J., Caviness, V. S., & Biederman, J. (2005). Structural brain magnetic resonance imaging of limbic and thalamic volumes in pediatric bipolar disorder. *The American journal of psychiatry*, *162*(7), 1256–1265. https://doi.org/10.1176/appi.ajp.162.7.1256

Goldstein, J. M., Seidman, L. J., Makris, N., Ahern, T., O'Brien, L. M., Caviness, V. S., Jr, Kennedy, D. N., Faraone, S. V., & Tsuang, M. T. (2007). Hypothalamic abnormalities in schizophrenia: sex effects and genetic vulnerability. *Biological psychiatry*, *61*(8), 935–945. https://doi.org/10.1016/j.biopsych.2006.06.027

Guerrero-Gonzalez, J., Surgent, O., Adluru, N., Kirk, G. R., Dean Iii, D. C., Kecskemeti, S. R., Alexander, A. L., & Travers, B. G. (2022). Improving Imaging of the Brainstem and Cerebellum in Autistic Children: Transformation-Based High-Resolution Diffusion MRI (TiDi-Fused) in the Human Brainstem. *Frontiers in integrative neuroscience*, *16*, 804743. https://doi.org/10.3389/fnint.2022.804743

Guerrero, J. M., Adluru, N., Bendlin, B. B., Goldsmith, H. H., Schaefer, S. M., Davidson, R. J., Kecskemeti, S. R., Zhang, H., & Alexander, A. L. (2019). Optimizing the intrinsic parallel diffusivity in NODDI: An extensive empirical evaluation. *PloS one*, *14*(9), e0217118. https://doi.org/10.1371/journal.pone.0217118

Han, X., Jovicich, J., Salat, D., van der Kouwe, A., Quinn, B., Czanner, S., Busa, E., Pacheco, J., Albert, M., Killiany, R., Maguire, P., Rosas, D., Makris, N., Dale, A., Dickerson, B., & Fischl, B. (2006). Reliability of MRI-derived measurements of human cerebral cortical thickness: the effects of field strength, scanner upgrade and manufacturer. *Neuroimage, 32*, 180-194.

Hua, K., Zhang, J., Wakana, S., Jiang, H., Li, X., Reich, D. S., Calabresi, P. A., Pekar, J. J., van Zijl, P. C. M., & Mori, S. (2008). Tract probability maps in stereotaxic spaces: Analyses of white matter anatomy and tract-specific quantification. *NeuroImage*, *39*(1), 336-347. https://doi.org/10.1016/j.neuroimage.2007.07.053

Iglesias, J.E., Augustinack, J.C., Nguyen, K., Player, C.M., Player, A., Wright, M., Roy, N., Frosch, M.P., Mc Kee, A.C., Wald, L.L., Fischl, B., and Van Leemput, K. (2015). A computational atlas of the hippocampal formation using ex vivo, ultra-high resolution MRI: Application to adaptive segmentation of in vivo MRI. *Neuroimage*, *115*, 117-137.

Jelescu, I. O., Veraart, J., Adisetiyo, V., Milla, S. S., Novikov, D. S., & Fieremans, E. (2015). One diffusion acquisition and different white matter models: how does microstructure change in human early development based on WMTI and NODDI?. *NeuroImage*, *107*, 242–256. https://doi.org/10.1016/j.neuroimage.2014.12.009

Jenkinson, M., Beckmann, C. F., Behrens, T. E., Woolrich, M. W., & Smith, S. M. (2012). FSL. *NeuroImage*, *62*(2), 782–790. https://doi.org/10.1016/j.neuroimage.2011.09.015

Jensen, J. H., & Helpern, J. A. (2010). MRI quantification of non-Gaussian water diffusion by kurtosis analysis. *NMR in Biomedicine*, *23*(7), 698–710. https://doi.org/10.1002/nbm.1518

Jensen, J. H., Helpern, J. A., Ramani, A., Lu, H., & Kaczynski, K. (2005). Diffusional kurtosis imaging: The quantification of non-gaussian water diffusion by means of magnetic resonance imaging. *Magnetic Resonance in Medicine*, *53*(6), 1432–1440. https://doi.org/10.1002/mrm.20508

Jones, D. K., & Leemans, A. (2011). Diffusion tensor imaging. *Methods in molecular biology (Clifton, N.J.)*, *711*, 127–144. https://doi.org/10.1007/978-1-61737-992-5_6

Jovicich, J., Czanner, S., Greve, D., Haley, E., van der Kouwe, A., Gollub, R., Kennedy, D., Schmitt, F., Brown, G., Macfall, J., Fischl, B., & Dale, A. (2006). Reliability in multi-site structural MRI studies: effects of gradient non-linearity correction on phantom and human data. *Neuroimage, 30*, 436-443.

Klein, A., & Tourville, J. (2012). 101 labeled brain images and a consistent human cortical labeling protocol. *Frontiers in neuroscience*, *6*, 171. https://doi.org/10.3389/fnins.2012.00171

Kuperberg, G.R., Broome, M.R., McGuire, P.K., David, A.S., Eddy, M., Ozawa, F., Goff, D., West, W.C., Williams, S.C., van der Kouwe, A.J., Salat, D.H., Dale, A.M., & Fischl, B. (2003). Regionally localized thinning of the cerebral cortex in schizophrenia. *Arch Gen Psychiatry, 60*, 878-888.

Le Bihan, D., Mangin, J. F., Poupon, C., Clark, C. A., Pappata, S., Molko, N., & Chabriat, H. (2001). Diffusion tensor imaging: concepts and applications. *Journal of magnetic resonance imaging : JMRI*, *13*(4), 534–546. https://doi.org/10.1002/jmri.1076

Lee, J. E., Chung, M. K., Lazar, M., DuBray, M. B., Kim, J., Bigler, E. D., Lainhart, J. E., & Alexander, A. L. (2009). A study of diffusion tensor imaging by tissue-specific, smoothing-compensated voxel-based analysis. *NeuroImage*, *44*(3), 870–883. https://doi.org/10.1016/j.neuroimage.2008.09.041

Liu, Z., Cheng, J., Zhu, H., Zhang, J., & Liu, T. (2020). Medical Image Computing and Computer Assisted Intervention – MICCAI 2020, 23rd International Conference, Lima, Peru, October 4–8, 2020, Proceedings, Part VII. Lecture Notes in Computer Science, 198–207. doi: 10.1007/978-3-030-59728-3_20

Makris, N., Goldstein, J. M., Kennedy, D., Hodge, S. M., Caviness, V. S., Faraone, S. V., Tsuang, M. T., & Seidman, L. J. (2006). Decreased volume of left and total anterior insular lobule in schizophrenia. *Schizophrenia research*, *83*(2-3), 155–171. https://doi.org/10.1016/j.schres.2005.11.020

Mori S, Oishi K, Jiang H, et al. (2008) Stereotaxic white matter atlas based on diffusion tensor imaging in an ICBM template. *Neuroimage, 40(2),* 570–582. doi:10.1016/j.neuroimage.2007.12.035

Nazeri, A., Schifani, C., Anderson, J. A. E., Ameis, S. H., & Voineskos, A. N. (2020). In Vivo Imaging of Gray Matter Microstructure in Major Psychiatric Disorders: Opportunities for Clinical Translation. *Biological psychiatry. Cognitive neuroscience and neuroimaging*, *5*(9), 855–864. https://doi.org/10.1016/j.bpsc.2020.03.003

Qi, X., & Arfanakis, K. (2021). Regionconnect: Rapidly extracting standardized brain connectivity information in voxel-wise neuroimaging studies. *NeuroImage*, *225*, 117462. https://doi.org/10.1016/j.neuroimage.2020.117462

Reuter, M., Schmansky, N.J., Rosas, H.D., Fischl, B. (2012). Within-Subject Template Estimation for Unbiased Longitudinal Image Analysis. *Neuroimage, 61 (4),* 1402-1418.

Reuter, M., Rosas, H.D., Fischl, B. (2010). Highly Accurate Inverse Consistent Registration: A Robust Approach. *Neuroimage, 53 (4),* 1181–1196.

Rosas, H.D., Liu, A.K., Hersch, S., Glessner, M., Ferrante, R.J., Salat, D.H., van der Kouwe, A., Jenkins, B.G., Dale, A.M., & Fischl, B. (2002). Regional and progressive thinning of the cortical ribbon in Huntington's disease. *Neurology, 58*, 695-701.

Salat, D.H., Buckner, R.L., Snyder, A.Z., Greve, D.N., Desikan, R.S., Busa, E., Morris, J.C., Dale, A.M., & Fischl, B. (2004). Thinning of the cerebral cortex in aging. *Cereb Cortex, 14*, 721-730.

Saygin ZM & Kliemann D (joint 1st authors), Iglesias JE, van der Kouwe AJW, Boyd E, Reuter M, Stevens A, Van Leemput K, Mc Kee A, Frosch MP, Fischl B, Augustinack JC. (2017). High-resolution magnetic resonance imaging reveals nuclei of the human amygdala: manual segmentation to automatic atlas. *Neuroimage*, *155*, 370-382.

Segonne, F., Dale, A.M., Busa, E., Glessner, M., Salat, D., Hahn, H.K., & Fischl, B. (2004). A hybrid approach to the skull stripping problem in MRI. *Neuroimage, 22*, 1060-1075.

Segonne, F., Pacheco, J., Fischl, B. (2007). Geometrically accurate topology-correction of cortical surfaces using nonseparating loops. *IEEE Trans Med Imaging, 26*, 518-529.

Sled, J.G., Zijdenbos, A.P., Evans, A.C. (1998). A nonparametric method for automatic correction of intensity nonuniformity in MRI data. *IEEE Trans Med Imaging, 17*, 87-97.

Stejskal E.O., & Tanner, J.E. (1965) Spin diffusion measurements: Spin echoes in the presence of a time-dependent field gradient. *J. Chem. Phys., 42,* 288.

Surgent, O., Riaz, A., Ausderau, K. K., Adluru, N., Kirk, G. R., Guerrero-Gonzalez, J., Skaletski, E. C., Kecskemeti, S. R., Dean Iii, D. C., Weismer, S. E., Alexander, A. L., & Travers, B. G. (2022).

Brainstem white matter microstructure is associated with hyporesponsiveness and overall sensory features in autistic children. *Molecular autism*, *13*(1), 48. https://doi.org/10.1186/s13229-022-00524-3

Tournier, J. D., Smith, R., Raffelt, D., Tabbara, R., Dhollander, T., Pietsch, M., Christiaens, D., Jeurissen, B., Yeh, C. H., & Connelly, A. (2019). MRtrix3: A fast, flexible and open software framework for medical image processing and visualisation. *NeuroImage*, *202*, 116137. https://doi.org/10.1016/j.neuroimage.2019.116137

Wakana, S., Caprihan, A., Panzenboeck, M. M., Fallon, J. H., Perry, M., Gollub, R. L., Hua, K., Zhang, J., Jiang, H., Dubey, P., Blitz, A., van Zijl, P., & Mori, S. (2007). Reproducibility of quantitative tractography methods applied to cerebral white matter. *NeuroImage*, *36*(3), 630-644. https://doi.org/10.1016/j.neuroimage.2007.02.049

Whitman, E. T., Elliott, M. L., Knodt, A. R., Abraham, W. C., Anderson, T. J., Cutfield, N. J., Hogan, S., Ireland, D., Melzer, T. R., Ramrakha, S., Sugden, K., Theodore, R., Williams, B. S., Caspi, A., Moffitt, T. E., & Hariri, A. R. (2025). DunedinPACNI estimates the longitudinal Pace of Aging from a single brain image to track health and disease. *Nature aging, 5(*8), 1619–1636. https://doi.org/10.1038/s43587-025-00897-z PMID: 40595015

Yin, C., Imms, P., Cheng, M., Amgalan, A., Chowdhury, N. F., Massett, R. J., Chaudhari, N. N., Chen, X., Thompson, P. M., Bogdan, P., Irimia, A., & Alzheimer's Disease Neuroimaging Initiative (2023). Anatomically interpretable deep learning of brain age captures domain-specific cognitive impairment. *Proceedings of the National Academy of Sciences of the United States of America*, *120*(2), e2214634120. https://doi.org/10.1073/pnas.2214634120 PMID: 36595679

Zhang, H., Schneider, T., Wheeler-Kingshott, C. A., & Alexander, D. C. (2012). NODDI: practical in vivo neurite orientation dispersion and density imaging of the human brain. *NeuroImage*, *61*(4), 1000–1016. https://doi.org/10.1016/j.neuroimage.2012.03.072

Zhang, S., Arfanakis, K. (2018). Evaluation of standardized and study-specific diffusion tensor imaging templates of the adult human brain: Template characteristics, spatial normalization accuracy, and detection of small inter-group FA differences. *Neuroimage, 172,* 40-50.

Zhang, Y., Brady, M., & Smith, S. (2001). Segmentation of brain MR images through a hidden Markov random field model and the expectation-maximization algorithm. *IEEE transactions on medical imaging*, *20*(1), 45–57. https://doi.org/10.1109/42.906424